fluids

MDPI

Article

Turbulence Characteristics of the Flexible Circular Cylinder Agitator

Sharul Sham Dol [1,*], Tshun Howe Yong [2], Hiang Bin Chan [2], Siaw Khur Wee [2] and Shaharin Anwar Sulaiman [3]

[1] Mechanical Engineering Department, Abu Dhabi University, P.O. Box 59911, Abu Dhabi 59911, United Arab Emirates
[2] Faculty of Engineering and Science, Curtin University Malaysia, CDT 250, Miri 98009, SWK, Malaysia; tshun.howe@postgrad.curtin.edu.my (T.H.Y.); hiang.bin@postgrad.curtin.edu.my (H.B.C.); wee.siaw.khur@curtin.edu.my (S.K.W.)
[3] Department of Mechanical Engineering, Universiti Teknologi PETRONAS, Tronoh 32610, PRK, Malaysia; shaharin@utp.edu.my
* Correspondence: sharulshambin.dol@adu.ac.ae

Abstract: A flexible protruding surface was employed as the flow disturbance to promote turbulence at the area of interest. An ultrasonic velocity profiler, UVP technique, was used to study the mean and fluctuating flow properties in the near wake of the rigid and flexible protruding surface in a water tunnel. The polymer based, ethylene-vinyl acetate (EVA) with an aspect ratio of AR = 10, 12, 14, 16 was used as the flexible circular cylinder, and submerged in a flow at Re = 4000, 6000 and 8000. The motion of the cylinder altered the fluid flow significantly. As a means to quantify turbulence, the wakes regions and production terms were analyzed. In general, the flexible cylinders show better capability in augmenting the turbulence than the rigid cylinder. The results show that the turbulence production term generated by the flexible cylinder is higher than that of rigid cylinder. The localized maximum shear production values have increased significantly from 131%, 203% and 94% against their rigid counterparts of AR = 16 at the Re = 4000, 6000 and 8000, respectively. The performance of turbulence enhancement depends heavily on the motion of the cylinder. The findings suggest that the turbulence enhancement was due to the oscillation of the flexible cylinder. The results have concluded that the flexible cylinder is a better turbulence generator than the rigid cylinder, thus improving the mixing of fluid through augmented turbulent flow.

Keywords: downwash; flexible circular cylinder; turbulence production; ultrasonic velocity profiler; upwash; wakes

Citation: Dol, S.S.; Yong, T.H.; Chan, H.B.; Wee, S.K.; Sulaiman, S.A. Turbulence Characteristics of the Flexible Circular Cylinder Agitator. *Fluids* **2021**, *6*, 238. https://doi.org/10.3390/fluids6070238

Academic Editors: Mehrdad Massoudi and Dimitrios V. Papavassiliou

Received: 9 April 2021
Accepted: 8 June 2021
Published: 30 June 2021

1. Introduction

Turbulence has always been and will always be a topic of interest in fluid dynamics. Many industries such as chemical, petro-chemical, natural gas processing, semi-conductor, thermal power plants and food process industries are benefiting from the characteristics of turbulence in part of their operations. Examples of turbulence characteristics include irregularity, diffusivity and rationality, in which they promote the mixing of fluids through the rate of momentum, mass and energy transports.

It is understood that the augmented turbulence is primarily due to the stronger and coherent vortices [1,2]. Researchers tend to favor the concept of passive control in mixing enhancement discussed in [3,4] because of the stronger vortices generated by the protruding surface under certain geometries [5]. Although the protruding surface can indeed generate vortices, the fact that it is essentially a rigid bluff body suggests that it also inevitably dissipates energy of the flow.

The biggest downside of a rigid structure is that the response to flow is not dynamics. A geometry with a higher angle of attack (e.g., cylinder, flat plate or blunt object of any shape) is needed if a higher level of turbulence is favored. Hence, compromising between

the turbulence level and pressure loss is necessary when designing the geometry. A smart memory alloy (SMA) based protruding surface for instance has the ability to vary its angle of attack to enhance turbulence or minimize pressure loss through temperature change [6,7].

Inspired by the ingenious SMA based protruding surface, the present work proposes to replace a conventional rigid protruding surface with a flexible protruding surface that has the ability to oscillate passively based on the incoming flow. Through the oscillation of the protruding flexible, the wasted energy "absorbed" by the rigid protruding surface is able to return to the flow by altering the flow dynamics. Therefore, the adoption of a flexible protruding surface could eliminate the probability of pairing with an external energy supply. Initial experimental work has been presented in [8].

The problem with the finite cylinder is complicated as not only are the free end conditions hard to predict, the base of the cylinder, known as the cylinder wall junction, is also susceptible to the boundary layer of the oncoming flow. The flow in this particular region has been studied in [9,10]. Okamoto and Yagita [11], Park and Lee [12] and Roh and Park [13] have studied the influence of end effects to the flow experimentally. They concluded that the central region that is free from the end effects starts to form at $AR > 3$. As the AR increases until $AR = 20$, the influence of end effects are so small that they can be considered to be two-dimensional [14].

The end effects of a finite cylinder are highly dependent on the AR of the cylinder and also the boundary layer thickness on the ground plane, as the reattachment of the separated flow can be influenced by those parameters. Though there are quite a few researchers actively involved in the research of end effects, the flow structure in this region remains speculative and needs additional experiments or simulations to verify their existence or structure, particularly the origin of the side-tip or trailing vortices. Despite the inconclusive results for detailed flow structure, it has been proven that the tip vortices are much stronger than the base vortices [15]. This further motivates the study of the finite cylinder as the flexible structure to enhance the strength of the vortices as opposed to the infinite cylinder.

When a free end of the finite cylinder, which has an AR greater than the critical AR, is exposed to the oncoming flow, there is a pair of counter-rotating trailing vortices which exists near the tip. The formation of these vortices is due to a phenomenon called upwash, which the upstream flow is associated with a weak upward-directed local velocity field at the free end, as reported by [16]. As the flow passes over the free end, downwash happens when the flow is brought down into the low-pressure region, immediately behind the cylinder [8]. The combination of the upwash flow on the side and downwash flow at the center interacts to form two counter-rotating trailing vortices [17], as shown in Figure 1. Furthermore, [10] reported that the part of the oncoming flow near the base moves downwards as it nears the cylinders and recirculates upstream of the cylinder-wall junction. It is there where the horseshoe vortex is formed and loops around the cylinder in the downstream direction. Park and Lee [12] also reported the similar flow pattern in their experimental results during their investigation on circular cylinders with $AR = 6$, 10 and 13 at $Re = 2 \times 10^4$ and 7.5×10^3.

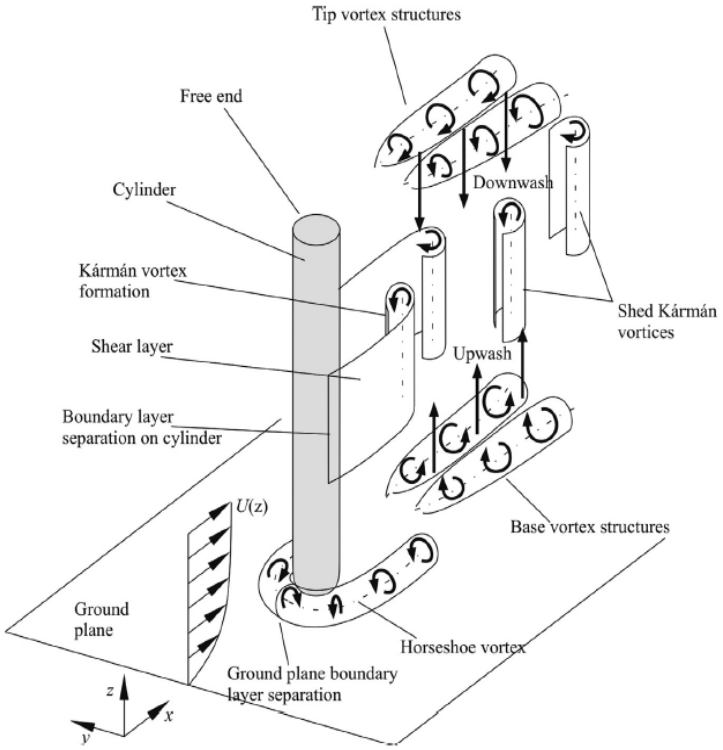

Figure 1. Schematic diagram of the flow field for finite circular cylinders greater than the critical aspect ratio. (Reproduced with permission from [18], published by Elsevier 2013.)

The flow structure for the finite cylinder with lower *AR* shows a drastic change in the wake structure. That distinct wake structure has been referred to as the arch vortex or mushroom vortex. As shown in the schematic (Figure 2) by [19], the oncoming flow separates from the leading edge of the cylinder's free end and a recirculation zone forms on top of the free end surface. There is a reversed flow at the center line of the free end surface. However, the results from [20] showed no trailing vortices and Kármán vortices associated with the arch vortex.

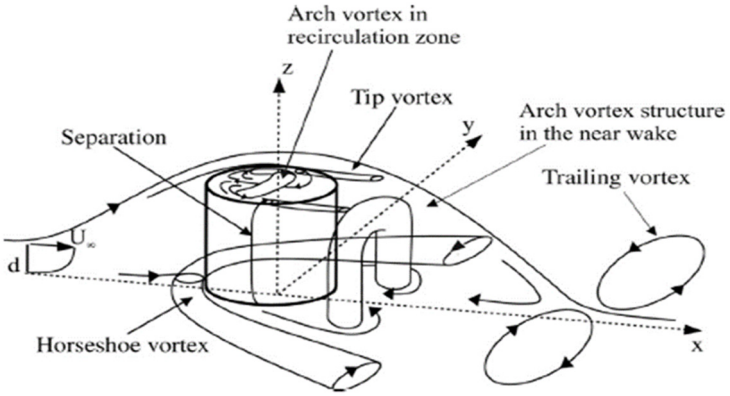

Figure 2. Schematic diagram of arch vortex formation for finite cylinders lower than the critical aspect ratio. (Reproduced with permission from [19], published by Springer Nature 2005.)

There is a need to understand how the structural mechanism affects the turbulence enhancement if the flexible protruding surface does indeed help in augmenting the turbulence level. The main objective is to experimentally investigate the turbulence enhancement of a single-phase flow by the flexible protruding surface, with the Reynolds number ranging within the subcritical flow regime. The velocity field profile from the near wake and production term are studied to quantify the turbulence characteristics.

2. Materials and Methods

A description of the water tunnel and its flow quality are described here. Detailed information on the ultrasonic velocity profiler (UVP) and the transducer, which were the velocity measurement techniques used, are also presented. A detailed set-up of the experiments with a schematic diagram are discussed, followed by the post-processing procedure, which is the kinetic energy budget method. Finally, a detailed uncertainty analysis of measurements and results parameters are presented.

2.1. Water Tunnel

Experiments were performed in the circulating open channel water tunnel placed at the Turbo Machine Laboratory, Universiti Teknologi PETRONAS as shown in Figure 3. The details and dimensions of the channel were reported in [8]. The test section where the measurements were conducted was installed with tempered glass on one of the side walls, for the flow visualization as well as allowing probes fixation. The water tunnel was equipped with a 1200 L/m end suction pump of 7.5 hp 440 VAC 3 phase capacity pump that was coupled with a Toshiba Inverter velocity controller. A maximum speed of 0.75 m/s was chosen as a higher pump speed could lead to more vigorous vibrations and increase the water temperature significantly. A poly-tube hexagonal honeycomb section was used as a flow straightener to reduce the turbulence intensity to no more than 7% [8].

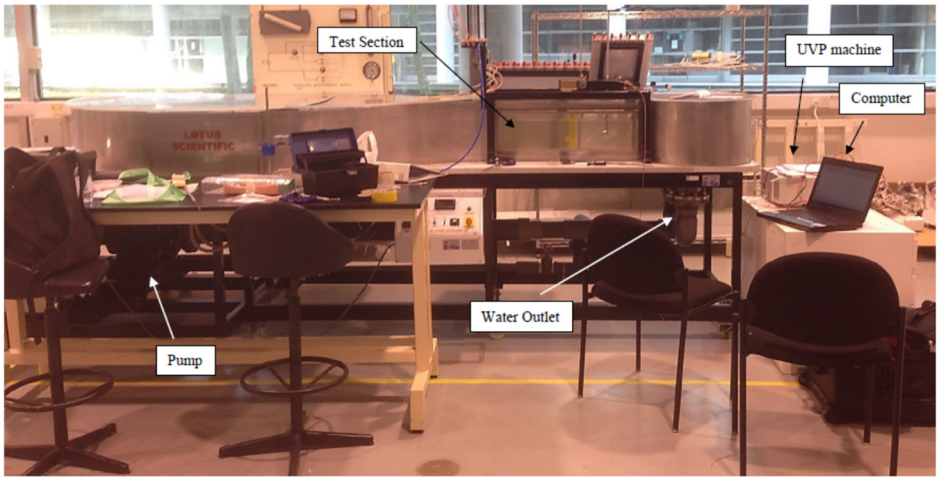

Figure 3. The water tunnel with the test section made of plexiglass for visualization purposes.

The velocity profile across the testing section was taken using a UVP by MET-FLOW. The time-average freestream velocity profile was averaged from 3000 samples. An incident angle of 30° of the transducer was projected into the water from the surface. The mean velocity profiles collapsed onto a common point indicating a fully developed boundary layer, as shown in Figure 4. All the cylinders were only partially immersed in the boundary layer, ensuring the free end was free from the boundary layer effect.

2.2. Ultrasonic-Velocity Profiler

The velocity profile across the testing section was obtained using an Ultrasonic Velocity Profiler by MET-FLOW (shown in Figure 5). A low frequency transducer, 2 MHz, was used owing to its ability to measure long distance and large velocity. The 2 MHz transducer is made of stainless-steel casing and has an outer diameter of 13 mm. The detailed working principle of the method is described in [21].

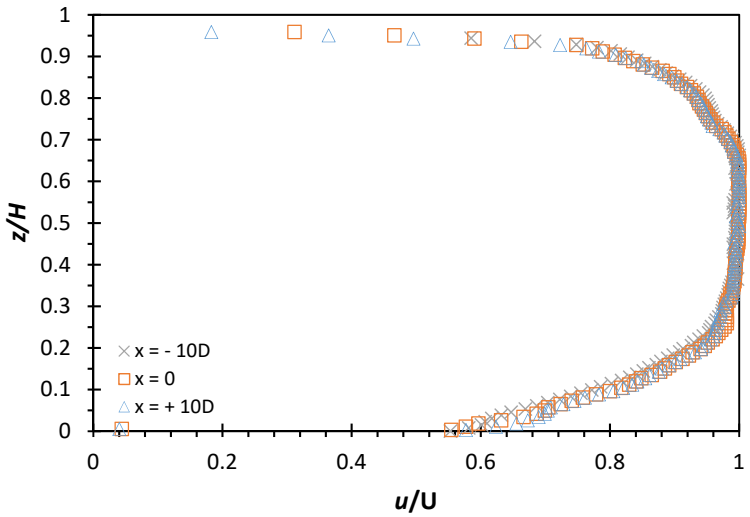

Figure 4. The mean velocity profiles at three different locations at a freestream velocity of $U = 0.65$ m/s.

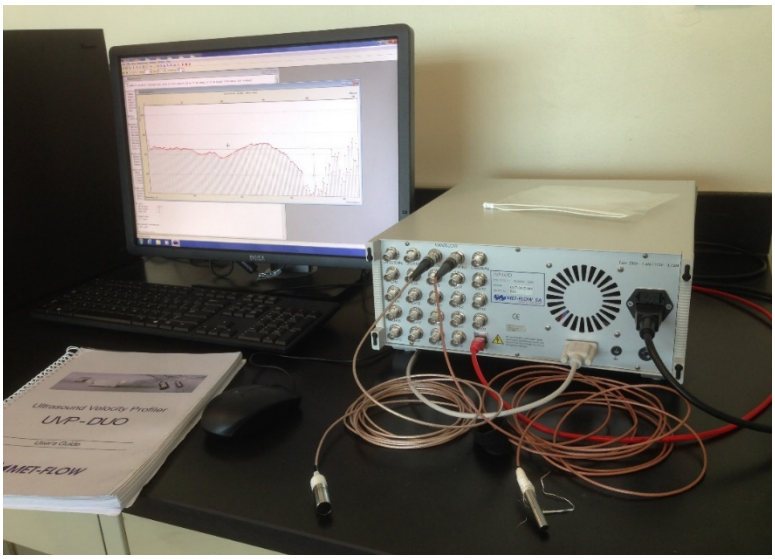

Figure 5. UVP machine from MET-FLOW.

The UVP uses the pulsed ultrasonic Doppler effect together with the echography relationship. The UVP transducer emits an ultrasound pulse into the liquid and the echoes are received by the same transducer. The time duration between the pulse emission and the instant of echo reception enables the transducer to calculate each position information of the fluid particle. The velocity information, on the other hand, is derived from the instantaneous Doppler shift frequency at that instant. The final form of the equation which is based on the Doppler shift frequency method can be written as below:

$$v = \frac{cf_d}{2f_0} \tag{1}$$

where v is the speed of the particle, c is the speed of sound in propagation medium, f_d is the detected Doppler shift frequency and f_0 is the frequency emitted by the transducer.

However, when used in conjunction with the transducer, one must account for the trajectory angle α called the Doppler angle as the transducer is always placed into the experimental system at an angle.

The UVP is capable of measuring either one velocity component or two and three velocity components. During the event of one velocity component measurement, one trans-

ducer is sufficient owing to its linewise measuring capability. However, when measuring two or three velocity components, more than one transducer is needed [22]. This is because each transducer is needed to measure each velocity component at one spatial point in order to form a vector. The vector is therefore obtained from any two non-parallel measured components. As the vector component is an orthogonal projection of a true vector into a measuring line, a large projection angle in between the two transducers is encouraged to avoid large inaccuracy in direction estimation. In other words, two-dimensional flow or three-dimensional flow measurements, unlike the technique of one-dimensional flow measurements, rely solely on the orthogonal composition technique which in turn can only be achieved at their respective intersection points. They concluded that in the test of one-dimensional flow, the error was estimated to be 2.5% to about 7% depending on the incident angle of the transducer. The results show that a smaller incident angle gives a higher error. Nevertheless, it shows the high accuracy of a single transducer in measuring one-dimensional flow. However, the results of two-dimensional flow measured by a single transducer deviate significantly. With that in mind, the projection angle between two transducers is orthogonal (90° in between the two transducers) when measuring the u and w velocity components behind the finite cylinder (see Figure 6). The use of UVP in measuring complex flow fields [23] and also the coherent structures in the near field of an axisymmetric jet [24] further prove the capability of UVP in handling a complex flow with confidence.

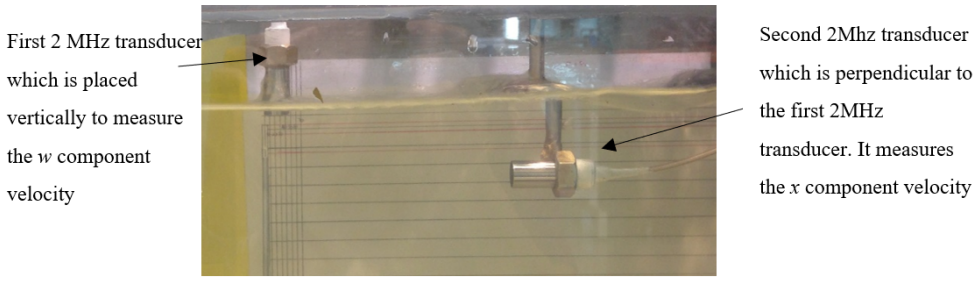

Figure 6. UVP transducers set-up at 90° to each other.

Speed calculations based on Doppler shift measurements are only possible if the Doppler angle is specified. Since the flow direction of the freestream is known (thereby assuming that the flow is fully one-dimensional), the Doppler angle can be predicted easily with only one transducer. The calibration of the 2 MHz transducer was carried by positioning it at a trajectory angle that has the minimum Doppler angle error possible which is used in speed calculations. The Doppler at large angles is more critical than it is at small angles in error estimation because the frequency shift becomes very small at large angles and the system sensitivity is reduced [25]. Nevertheless, three sets of measurements with different trajectory angles of 20°, 30° and 40° were conducted in the investigation of the freestream quality and each set of trajectory angle was repeated three times. It was found from the mean velocity profiles that the differences of the profiles measured from the trajectory angle of 20° and 30° were negligible, though the repeatability of the trajectory angle of 30° was better. As a result, the trajectory angle of 30° was used. A 256 pulse of repetitions was selected throughout the experiments (one velocity profile is determined after 256 repetitions whereby the repetition represents the number of samples the echo signals reflected, which the system uses to reconstruct the Doppler frequency correctly). A sampling rate of 1 kHz was used in obtaining 3000 samples of the profiles. The spatial resolution was 1.47 mm.

2.3. Flexible Circular Cylinders

As for the experiments of finite flexible circular cylinders, it was separated into two categories by the choice of materials: metal and polymer. Under the category of metal,

the aluminum cylinder and carbon steel cylinders were used; whereas, an Ethylene vinyl acetate (EVA) cylinder was chosen for the category of polymer.

The diameter of the aluminum and carbon steel cylinder was $D = 3.0 \pm 0.5$ mm (see Ref [8]). Two $AR = 50$ and 54 of the aluminum and carbon steel cylinders were investigated in these experiments. The intentionally large AR was chosen for two reasons. First, the stiffness of metal is significantly higher than that of polymer. Thus, in order for the cylinder to experience vibration induced by the different pressures caused by the vortex shedding, the diameter and the length must be kept small and long. Second, the height was physically limited by the water tunnel dimensions. On the other hand, four EVA cylinders with diameters $D = 11.0 \pm 0.5$ mm and $AR = 10$, 12, 14 and 16 (see Figure 7 for $AR = 12$, $Re = 6000$) were used in these experiments. The blockage ratio was at most 1.2% for metal group models and 4.8% for polymer group models. The measurements were done at the following Reynolds numbers based on the diameter of the cylinders: $Re = 2500$ (metal group) and 4000, 6000 and 8000 (polymer group). A Reynolds number of $Re = 2500$ was selected for the metal group flexible cylinder because it was limited by the maximum freestream velocity available due to a very high U that was needed to achieve the same Re as the polymer group cylinder.

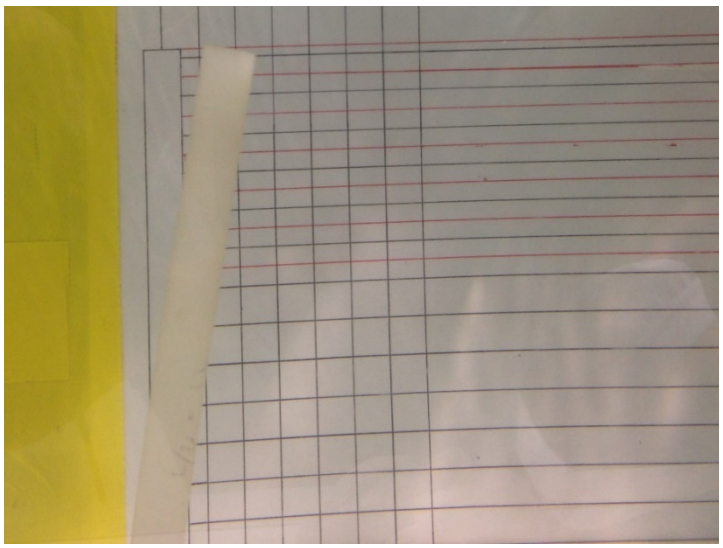

Figure 7. EVA flexible cylinders with $AR = 12$ and $Re = 6000$.

2.4. Descriptions of Experiments

Figure 8 shows the schematic diagram of the experimental set-up within the test section of the water tunnel. For each cylinder, the time-averaged velocity field $(\overline{U}, \overline{W})$ in the downstream (x-z plane) of the cylinder was measured over a 5 mm uniform grid over the top 5D span of the cylinder at streamwise locations of x/D = 1 to x/D = 5. The measurement point in the wall-normal direction (z plane) increased to a 10 mm uniform grid after the 5D span of the cylinder until it was 10 mm from the ground. As the tip effects are generally extended up to 3D to 4D from the free end [11–13], more attention was given to the free end until 5D along the cylinder span so that the tip effects could be captured. The measurement zone was free from the influence of the ground plane boundary layer for all cylinders. All the measurements were made at the y-z plane of symmetry.

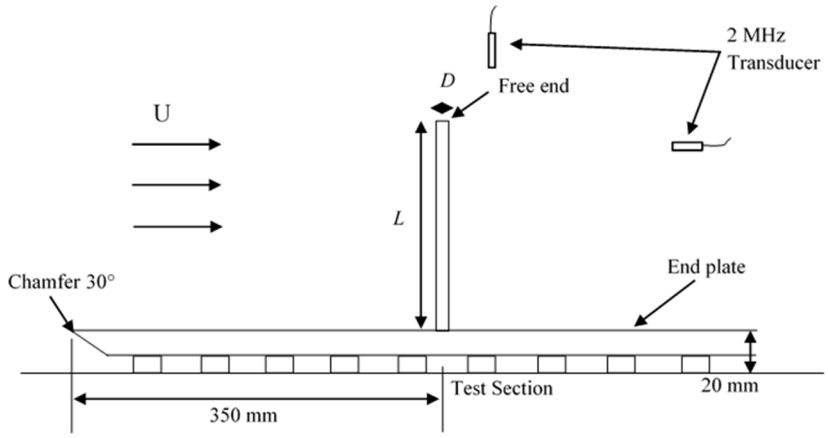

Figure 8. Schematic diagram of experimental set-up in the water tunnel.

2.5. Uncertainty Analysis

The uncertainty estimation for the different parameters was calculated based on the Coleman and Steele [26] approach at a 90% confidence level. Based on the approach, the summary of the uncertainty estimation in the freestream parameters and experimental model dimensions are presented in [8]. The uncertainty estimations for the results parameters are presented in Table 1.

Table 1. Summary of uncertainty estimation for results parameters.

Parameter	Uncertainty (%)
Angle of the Probe	±0.50
Streamwise Velocity Component, u	±4.67
Wall-normal Velocity Component, w	±4.82
Streamwise Turbulence Intensity, u'	±6.24
Wall-normal Turbulence Intensity, w'	±6.81
Reynolds shear stress, $\overline{u'w'}$	±8.36
Distance of Oscillation Acquired from Digital Recording	±3.37

The accuracy of the UVP was fairly adequate, with an associated velocity resolution of 0.4% of the velocity range. Therefore, a ± 0.4% of value obtained by the MET-FLOW UVP was accounted for and treated as a bias error that was always present in all the values obtained by MET-FLOW UVP throughout the experiments.

2.6. Kinetic Energy Budget

The behavior of fluctuation quantities can be described by applying the Reynolds decomposition method to the Navier–Stokes equations and after a series of simplifications [27] the kinetic energy budget which describes the energy of turbulence is formed. Since the kinetic energy budget provides insight on how the turbulence is distributed after being produced from the mean flow, there exists the kinetic energy budget for the mean flow and the kinetic energy budget for the turbulent flow, both of which compliment each other in the process of examining the transfer of turbulence energy. The kinetic energy budget of mean flow is given by:

$$\frac{D}{Dt}\left(\frac{1}{2}U_i^2\right) = \frac{\partial}{\partial x_j}\left(-\frac{PU_j}{\rho_o} + 2\nu U_i E_{ij} - \overline{u_i' u_j'} U_i\right) - 2\nu E_{ij}E_{ij} + \overline{u_i' u_j'}\frac{\partial U_i}{\partial x_j} - \frac{g}{\rho_o}\overline{\rho} U_3 \quad (2)$$

whilst the kinetic energy budget of turbulent flow is given by the following equation:

$$\frac{D}{Dt}\left(\overline{\frac{1}{2}u_i'^2}\right) = -\frac{\partial}{\partial x_j}\left(\frac{\overline{pu'_j}}{\rho_o} - 2\nu\overline{u_i' e_{ij}} + \frac{1}{2}\overline{u_i' u_i' u_j'}\right) - 2\nu\overline{e_{ij}e_{ij}} - \overline{u_i' u_j'}\frac{\partial U_i}{\partial x_j} + g\alpha\overline{\omega T'} \quad (3)$$

The production term $-\overline{u_i' u_j'} \frac{\partial U_i}{\partial x_j}$ is generally positive in the kinetic energy budget of turbulent flow, signifying an energy supply from the mean flow to the turbulent flow. When comparing the Equations (2) and (3), it can be understood that the transfer of energy between the mean and turbulent flow can only be done through the fifth term on the RHS, and therefore is often labelled as the production term.

The kinetic energy budget equations are useful in 'visualizing' the nature of turbulence and are especially useful in examining the level of turbulence energy produced by the rigid and flexible cylinders through evaluating the production term. In the current work, attention is given to the production term to understand the distribution of the energy by the rigid and flexible cylinders.

3. Results and Discussion

Yong et al. [28] investigated the time-averaged streamwise ($\overline{u}/U$) and wall-normal ($\overline{w}/U$) velocity profile of rigid and flexible finite cylinders of AR = 10 and 16 at Re = 4000, 6000 and 8000 and conclusively it can be seen that the diminishing/weakening of downwash has resulted in the increased height of the wake region in the case of the rigid cylinder. Thus, most of the vortices generated can be transported downstream instead of downwards. As most of the vortices generated are immediately transported downwards for the rigid cylinder, the wake region is smaller. As all of the turbulent activities happen within the wake, the region of the wake can serve as a preliminary indication to the amount of turbulence present behind an object (see Figure 9 for example). The turbulence enhancement associated to this oscillation is significant. Therefore, the results suggest that an organized oscillation with consistently high amplitude and frequency is important in enhancing the turbulence production. As a result, a consistent amplitude and frequency are very important in determining the turbulence production. The structural velocity graphs are all normalized by the freestream velocity so that the actual structural velocity by the cylinder against the freestream velocity is plain to see.

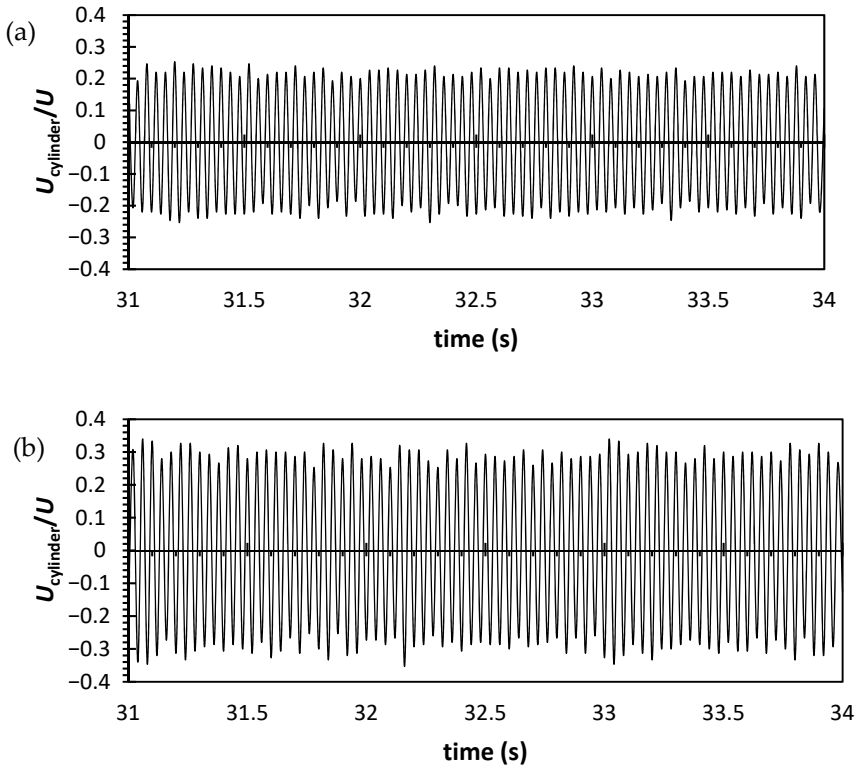

Figure 9. The normalized structural velocity of aluminum flexible cylinder at Re = 2500 in the y-direction (**a**) AR = 50; (**b**) AR = 54.

As discussed in [8,21], the influence of the tip effects for a rigid or flexible cylinder is up to 3*D* and insignificant diameters from the free end, respectively. This translates to a different size of wake behind the rigid and flexible cylinders. The size of the wake behind a flexible cylinder is greater than that of a rigid cylinder by circa 2*D* for the same *AR*. As the influence of a downwash phenomenon is very negligible behind a flexible cylinder, the tip vortex generated can be transported downstream more effectively without being downwashed towards the ground. Thus, the effective area of which the turbulent activities happen improves considerably. It is with substantial evidence that the wake region increment is achieved through the use of the flexible cylinder. However, there are two additional phenomena that are associated with the flexible cylinder: deflection in the *x*-direction and oscillation traverse to the flow. Therefore, the roles of these phenomena are examined in this paper.

It was discussed in Section 2.6 that the kinetic energy budget equations provide 'visualization' on how turbulence is spatially distributed after being produced in the mean flow. It is particularly useful to analyze the production term, $-\overline{u_i' u_j'} \frac{\partial U_i}{\partial x_j}$ (for convenience, it is thereby labelled as *P* throughout the context) to examine how much energy is contributed to the turbulence formation. Therefore, attention is put on this term as its relationships with the coherent structures present in the flow [29,30] and its evolution along the downstream location can provide adequate information such as when the turbulence energy starts to attenuate.

3.1. Production Term of Rigid Cylinders

The normalized production term graph downstream of the rigid cylinders of $AR = 10$ at $Re = 4000$, 6000 and 8000 are presented in Figure 10. As shown in the figures, the local maximum occurs in the vicinity of the free end of the rigid cylinders at $x/D = 2$. The localized P_{max} values of the rigid cylinders are approximately 0.035, 0.035 and 0.037 for $Re = 4000$, 6000 and 8000, respectively. There is a slight increment of turbulent energy production for the rigid cylinder at $Re = 8000$. The *P* value attenuates considerably quickly after $x/D = 3$, which is consistent with the downwash phenomena where it transports most of the vortices downwards.

The rigid cylinders of $AR = 16$ (see Figure 11) on the other hand, also spot a similar observation where the P_{max} occurs near the free end of the rigid cylinders at $x/D = 2$. The localized P_{max} value is observed at 0.035, 0.036 and 0.039 for $Re = 4000$, 6000 and 8000. Similar to $AR = 10$, the *P* value at circa $z/D = AR$-2 is significantly lower than the span below due to the tip effects which is up to 3*D* from the free end, limiting the wake region to approximately 2*D*–3*D* below the free end of the cylinder.

As turbulence is an instability generated by shear, the stronger the shear is would ideally indicate a stronger turbulence. This is also evident from the shear production term equation, *P*, of the turbulent kinetic budget equations where the term is governed partly by the shear rate. Additionally, the localized P_{max} occurs in the vicinity of the free end of the rigid cylinders because that is the region where shear layer instability happens most dramatically, which then induces the roll-up phenomenon and later transfers the kinetic energy from the mean flow to the primary vortices. As the flow accelerates over the free end, the accelerated layer and the layer below it creates a strong shear region.

It would also seem that the *AR* plays no significant role in enhancing the turbulence production in the rigid cylinder case as both $AR = 10$ and 16 have a similar *p* value at the same *Re*. It is therefore suggested that the geometrical factor does not contribute to the turbulence enhancement.

3.2. Production Term of Flexible Cylinders

Figure 12 shows the normalized *P* graph of the flexible cylinders of $AR = 10$ at $Re = 4000$, 6000 and 8000. Similar observations of the rigid counterpart can be seen on the flexible cylinders of $AR = 10$ at $Re = 4000$ and 6000 as it has been established in the previous sub-chapter that the cylinders under these two *Re* conditions behave like a rigid cylinder.

Thus, it is expected to have a similar turbulence performance as the rigid counterpart. The flexible cylinder at Re = 8000, on the other hand, has spotted a slight increment of the localized $P_{\max}$ at 0.041 over its rigid counterpart at the same Re. Similarly, it also happens in the vicinity of the free end, where a large amount of shear occurs. The cylinder did oscillate but the oscillation was too minute to be registered.

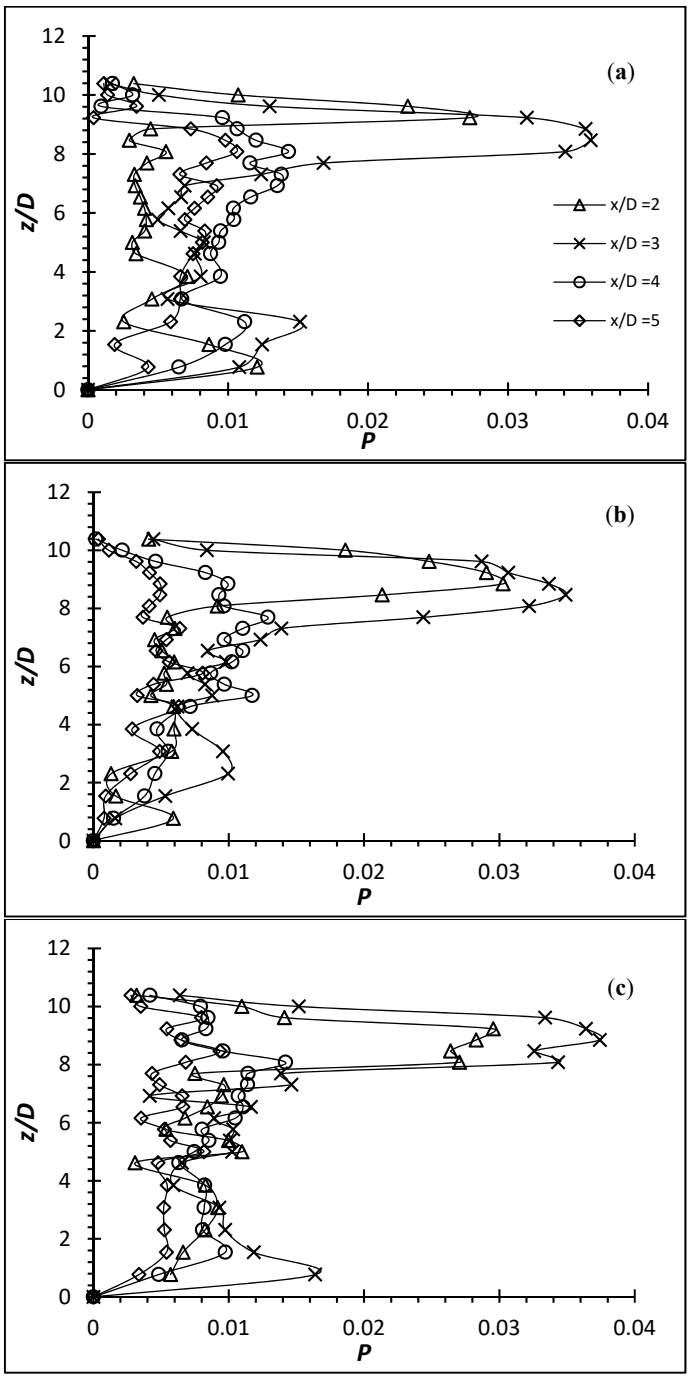

Figure 10. Production term $-\overline{u_i' u_j'} \frac{\partial U_i}{\partial x_j}$ for rigid cylinder of AR = 10 at (**a**) Re = 4000; (**b**) Re = 6000; (**c**) Re = 8000.

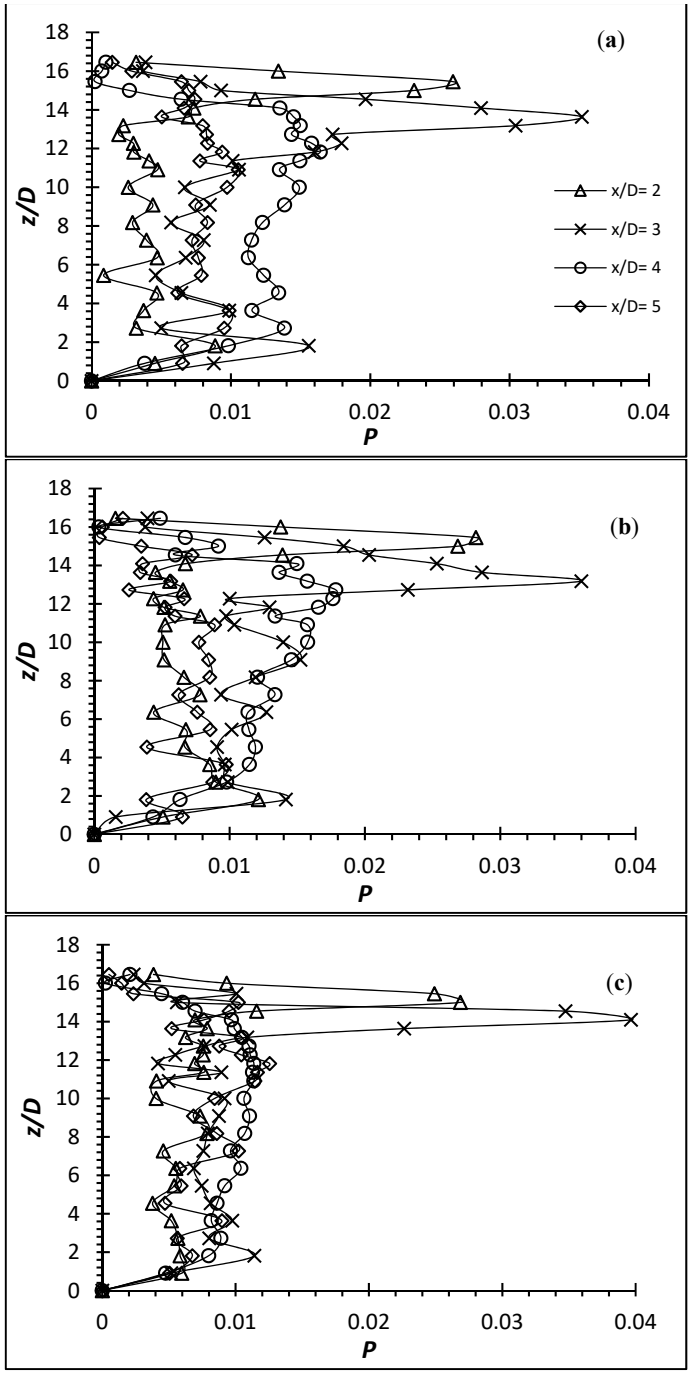

Figure 11. Production term $-\overline{u_i' u_j'} \frac{\partial U_i}{\partial x_j}$ for rigid cylinder of AR = 16 at (**a**) Re = 4000; (**b**) Re = 6000; (**c**) Re = 8000.

The normalized P graph of the flexible cylinders of AR = 16 at Re = 4000, 6000 and 8000 are presented in Figure 13. It is important to remind the readers again that due to the deflection of the flexible cylinders during the experiments, no measurement can be made in the near wake where the deflection interfered with the measurement points. In general, the localized $P_{\max}$ occurs near the free end, very similar to its rigid counterpart as it is where the region shear happens most. This indicates that the energy from the mean flow is transferred to the fluctuating flow through the mechanism of shear. The localized $P_{\max}$ of the flexible cylinders are 0.081, 0.109 and 0.076 for Re = 4000, 6000 and 8000, respectively. The localized $P_{\max}$ values have increased significantly from 131%, 203% and 94% against their rigid counterpart of AR = 16 at the same condition of Re, respectively.

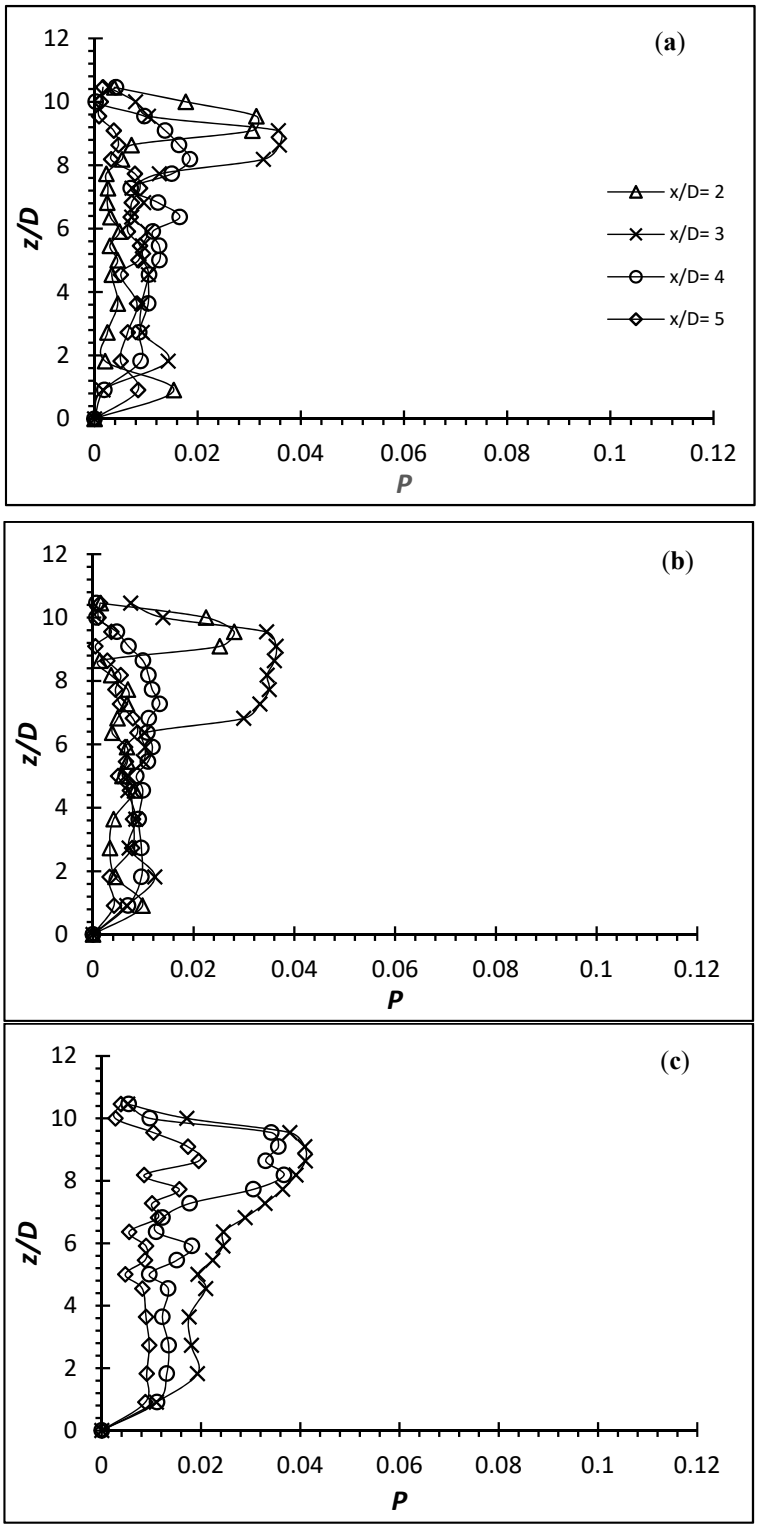

Figure 12. Production term $-\overline{u_i' u_j'} \frac{\partial U_i}{\partial x_j}$ for flexible cylinder of AR = 10 at (**a**) Re = 4000; (**b**) Re = 6000; (**c**) Re = 8000.

Apart from the obvious increment of localized $P_{\max}$ near the free end, it can also be discerned that the region below the free end has increased as well, compared to its rigid counterpart at the same localized region. The P value at the midspan of the cylinder at x/D = 3 and 4 has a modest improvement over its rigid counterpart. This suggests that the production of turbulent energy is slightly stronger than its rigid counterpart probably

due to the absence of downwash which limits most of the turbulence activities within the near wake.

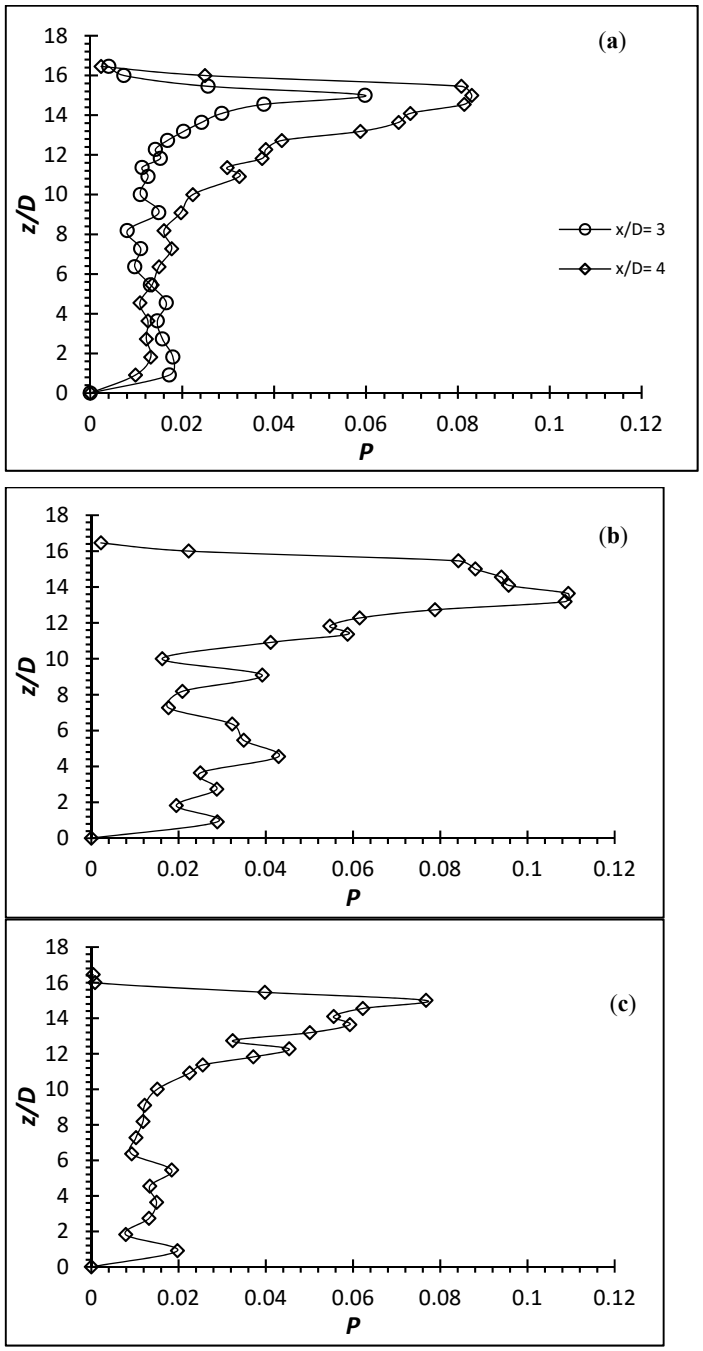

Figure 13. Production term $-\overline{u_i' u_j'} \frac{\partial U_i}{\partial x_j}$ for flexible cylinder of AR = 16 at (**a**) Re = 4000; (**b**) Re = 6000; (**c**) Re = 8000.

The turbulent performance is increased significantly at three different Re for the flexible cylinders. Since it is suggested by the results of the rigid cylinder that the geometry factor (increasing AR) does not contribute to the turbulent performance, the major value difference generated by the flexible cylinders at three different Re is believed to be caused by the structural dynamics factors (e.g., degree of deflection, oscillation frequency), which are heavily dependent on the AR. It is after all the increase in AR that results in the reduction of structural stiffness (provided the geometry and material used are consistent). Therefore, the increase in AR should make the cantilever experience a larger deflection and oscillation.

Conclusively, it is believed that the turbulent performance should be closely linked to the structural dynamics caused by different *AR* rather than the *AR* itself.

4. Conclusions

The streamwise, u, and wall-normal, w, components' flow behind the rigid and flexible finite cantilevers were investigated experimentally using UVP at Re = 2500, 4000, 6000 and 8000 with the goal of identifying the turbulence characteristics in the flow field caused by the flexible cantilevers. Each cylinder was mounted as normal to a ground plane and was partially immersed in a turbulent boundary layer. The aspect ratio of the rigid cylinder investigated was AR = 10 and 16. On the other hand, the flexible EVA cylinder and flexible metal-based cylinder was AR = 10, 12, 14 and 16 and AR = 50 and 54, respectively. In general, it is seen that the wake region behind the flexible cylinder is greater than the rigid cylinder. It is important to note that both the rigid and flexible cylinders were put into the same exact flow condition. An increase in the wake region indicates that the effective region of the turbulence activities is increased, leading to an improvement of the turbulence generation. This indicates that the flexible cylinder can indeed improve in the turbulence generation through expanding the effective turbulent region. The results also show that the P term generated by the flexible cylinder is higher than that of rigid cylinder.

Author Contributions: Conceptualization, H.B.C. and S.S.D.; methodology, T.H.Y. and S.A.S.; software, H.B.C.; validation, T.H.Y., S.S.D. and S.K.W.; formal analysis, T.H.Y. and S.S.D.; investigation, T.H.Y. and H.B.C.; resources, S.S.D. and S.A.S.; data curation, S.K.W.; writing—original draft preparation, T.H.Y. and S.S.D.; writing—review and editing, S.S.D.; visualization, T.H.Y.; supervision, S.S.D. and S.K.W.; project administration, S.S.D.; funding acquisition, S.S.D. All authors have read and agreed to the published version of the manuscript.

Funding: This research project was fully supported and funded by Fundamental Research Grant Scheme from Ministry of Higher Education Malaysia.

Conflicts of Interest: The authors declare no conflict of interest.

References

1. Dol, S.S. Weakened vortex shedding from a rotating cylinder. *Int. J. Mech. Mechatron. Eng.* **2013**, *7*, 2013–2020.
2. Dol, S.S. Proper orthogonal decomposition analysis of vortex shedding behind a rotating circular cylinder. *Eur. Phys. J. Conf.* **2016**, *114*, 02019. [CrossRef]
3. Lin, J.C. Review of research on low-profile vortex generators to control boundary-layer separation. *Prog. Aerosp. Sci.* **2002**, *38*, 389–420. [CrossRef]
4. Dol, S.S.; Chan, H.B.; Wee, S.K.; Perumal, K. The effects of flexible vortex generator on the wake structures for improving turbulence. *IOP Conf. Ser. Mater. Sci. Eng.* **2020**, *715*, 012070. [CrossRef]
5. Carletti, M.J.; Rogers, C.B.; Parekh, D.E. Parametric study of jet mixing enhancement by vortex generators, tabs, and deflector plates. *Asme-Publ.-Fed* **1996**, *237*, 303–312.
6. Aris, M.S.; Owen, I.; Sutcliffe, C.J. The development of active vortex generators from shape memory alloys for the convective cooling of heated surfaces. *Int. J. Heat Mass Transf.* **2011**, *54*, 3566–3574. [CrossRef]
7. Aris, M.S.; Owen, I.; Sutcliffe, C.J. The application of shape memory alloy as longitudinal vortex generators for enhanced convective heat transfer. In Proceedings of the 10th UK National Heat Transfer Conference, Edinburgh, UK, 10–11 September 2007.
8. Yong, T.H.; Chan, H.B.; Dol, S.S.; Wee, S.K.; Sulaiman, S.A. Experimental Investigation on Effects of Elastic Agitator to Turbulence Enhancement. *J. Appl. Fluid Mech.* **2021**, *14*, 361–373.
9. Agui, J.H.; Andreopoulos, J. Experimental Investigation of a ThreeDimensional Boundary Layer Flow in the Vicinity of an Upright Wall Mounted Cylinder (Data Bank Contribution). *J. Fluids Eng.* **1992**, *114*, 566–576. [CrossRef]
10. Graf, W.H.; Yulistiyanto, B. Experiments on Flow around a cylinder; the velocity and vorticity fields. *J. Hydraul. Res.* **1998**, *36*, 637–653. [CrossRef]
11. Okamoto, T.; Yagita, M. The experimental investigation on the flow past a circular cylinder of finite length placed normal to the plane surface in a uniform stream. *Bull. JSME* **1973**, *16*, 805–814. [CrossRef]
12. Park, C.W.; Lee, S.J. Free end effects on the near wake flow structure behind a finite circular cylinder. *J. Wind. Eng. Ind. Aerodyn.* **2000**, *88*, 231–246. [CrossRef]
13. Roh, S.; Park, S. Vortical flow over the free end surface of a finite circular cylinder mounted on a flat plate. *Exp. Fluids* **2003**, *34*, 63–67. [CrossRef]

14. Dol, S.S.; Kopp, G.A.; Martinuzzi, R.J. The suppression of periodic vortex shedding from a rotating circular cylinder. *J. Wind. Eng. Ind. Aerodyn.* **2008**, *96*, 1164–1184. [CrossRef]
15. Rostamy, N.; Sumner, D.; Bergstrom, D.J.; Bugg, J.D. Local flow field of a surface-mounted finite circular cylinder. *J. Fluids Struct.* **2012**, *34*, 105–122. [CrossRef]
16. Kawamura, T.; Hiwada, M.; Hibino, T.; Mabuchi, I.; Kumada, M. Flow around a Finite Circular Cylinder on a Flat Plate: Cylinder height greater than turbulent boundary layer thickness. *Bull. JSME* **1984**, *27*, 2142–2151. [CrossRef]
17. Kitagawa, T.; Fujino, Y.; Kimura, K.; Mizuno, Y. Wind pressures measurement on end-cell-induced vibration of a cantilevered circular cylinder. *J. Wind. Eng. Ind. Aerodyn.* **2002**, *90*, 395–405. [CrossRef]
18. Sumner, D. Flow above the free end of a surface-mounted finite-height circular cylinder: A review. *J. Fluids Struct.* **2013**, *43*, 41–63. [CrossRef]
19. Pattenden, R.J.; Turnock, S.R.; Zhang, X. Measurements of the flow over a low-aspect-ratio cylinder mounted on a ground plane. *Exp. Fluids* **2005**, *39*, 10–21. [CrossRef]
20. Lee, L.; Wang, Y. Aerodynamics of a circular cylinder of finite length in cross flow. In Proceedings of the Forum on Turbulent Flows 1987, Cincinnati, OH, USA, 14–17 June 1987; pp. 61–65.
21. Takeda, Y. Velocity profile measurement by ultrasonic Doppler method. *Exp. Therm. Fluid Sci.* **1995**, *10*, 444–453. [CrossRef]
22. Yokoyama, K.; Kashiwaguma, N.; Okubo, T.; Takeda, Y. Flow measurement in an open channel by UVP. *Proc. ISUD* **2004**, *4*, 204–210.
23. Kantoush, S.A.; De Cesare, G.; Boillat, J.L.; Schleiss, A.J. Flow field investigation in a rectangular shallow reservoir using UVP, LSPIV and numerical modelling. *Flow Meas. Instrum.* **2008**, *19*, 139–144. [CrossRef]
24. Inoue, Y.; Yamashita, S.; Kondo, K. Experiments in an Initial Region of a Circular Free Jet. In Proceedings of the 4th ISUD, Sapporo, Japan, 6–8 September 2004.
25. Dol, S.S.; Wong, S.F.; Wee, S.K.; Lim, J.S. Experimental Study on the Effects of Water-in-oil Emulsions to Wall Shear Stress in the Pipeline Flow. *J. Appl. Fluid Mech.* **2018**, *11*, 1309–1319. [CrossRef]
26. Coleman, H.W.; Steele, W.G. *Experimentation and Uncertainty Analysis for Engineers*, 2nd ed.; Wiley: New York, NY, USA, 1999.
27. Dol, S.S.; Salek, M.M.; Martinuzzi, R.J. Energy redistribution between the mean and pulsating flow field in a separated flow region. *J. Fluids Eng.* **2014**, *136*, 111105. [CrossRef]
28. Yong, T.H.; Chan, H.B.; Dol, S.S.; Wee, S.K.; Kumar, P. The flow dynamics behind a flexible finite cylinder as a flexible agitator. In *IOP Conference Series: Materials Science and Engineering*; IOP Publishing: Bristol, UK, 2017; Volume 206, p. 012033.
29. Haase, W.; Braza, M.; Revell, A. (Eds.) *DESider—A European Effort on Hybrid RANS-LES Modelling: Results of the European-Union Funded Project, 2004–2007*; Springer Science & Business Media: Berlin, Germany, 2009; Volume 103.
30. Dol, S.S.; Salek, M.M.; Martinuzzi, R.J. Effects of pulsation to the mean field and vortex development in a backward-facing step flow. *J. Fluids Eng.* **2014**, *136*, 011001. [CrossRef]